Earth and Planetary Science Letters 538 (2020) 116208

Contents lists available at ScienceDirect

Earth and Planetary Science Letters

www.elsevier.com/locate/epsl

Transfer of oxygen to Earth's core from a long-lived magma ocean

Christopher J. Davies [a,*], Monica Pozzo [b], David Gubbins [a], Dario Alfè [b,c]

[a] School of Earth and Environment, University of Leeds, Leeds LS2 9JT, UK
[b] Department of Earth Sciences and Thomas Young Centre @ UCL, UCL, Gower Street, WC1E 6BT, London, UK
[c] Dipartimento di Fisica Ettore Pancini, Università di Napoli Federico II, Monte S. Angelo, I-80126 Napoli, Italy

ARTICLE INFO

Article history:
Received 7 October 2019
Received in revised form 11 February 2020
Accepted 4 March 2020
Available online 16 March 2020
Editor: R. Dasgupta

Keywords:
Earth's core
stratified layer
chemical interactions
magma ocean

ABSTRACT

Chemical interactions between metal and silicates at the core-mantle boundary (CMB) are now thought to lead to transfer of oxygen into Earth's liquid core. Establishing the nature and extent of this transfer is important for constraining the conditions under which the core formed, the origin of a stably stratified region below the CMB and the possible precipitation of oxides within the core. Previous models of FeO transfer have considered a solid mantle; however, several lines of evidence suggest that the lowermost mantle could have remained above its solidus long after core formation was complete, which would allow much faster mass transfer. We investigate this scenario by developing a time-dependent model of FeO exchange between a diffusive stratified layer at the top of the core and a long-lived molten magma ocean. Core FeO concentration, $\bar{c}^c_{FeO}$, is evolved subject to a time-dependent mass flux at the CMB, radius $r_{\rm cmb}$, which depends on the FeO concentration at the bottom ($\bar{c}^m_{FeO}(r_{\rm cmb})$) and top ($\bar{c}^m_{FeO}(r_{\rm bulk})$) of the chemical boundary layer above the CMB. Coupled core-magma ocean evolution arises because $\bar{c}^m_{FeO}(r_{\rm cmb})$ and $\bar{c}^c_{FeO}(r_{\rm cmb})$ are linked through the partition coefficient $P = \bar{c}^c_{FeO}(r_{\rm cmb})/\bar{c}^m_{FeO}(r_{\rm cmb})$. $\bar{c}^m_{FeO}(r_{\rm bulk})$ is held constant in No Crystallization (NC) models and evolves in Middle-Out Crystallization (MOC) models according to the basal magma ocean model of Labrosse et al. (2007), generalised to account for FeO loss to the core. In the first 1 Gyr, FeO transfer in all models with $\geq 10\%$ FeO in the magma ocean and $P \geq 5$ produces pure FeO compositions at the CMB, stably stratified layers of $60-80$ km and accounts for $15-50\%$ of the total present-day core oxygen content. In NC models the magma ocean does not completely freeze in 4 Gyr, in which time the stable layer reaches $120-150$ km and FeO transfer can account for all of the present-day O in the core. However, in MOC models FeO loss to the core causes the magma ocean to completely freeze in the first 1-3 Gyrs following core formation. Our results suggest that the present-day core composition may not provide a strong constraint on models of core formation and that FeO could have precipitated at the top of the core.

1. Introduction

The manner in which elements partition between silicates and metals at high pressure and temperature is critical for determining the structure, dynamics and evolution of the terrestrial planets. Equilibrium conditions during differentiation of these bodies some 4.5 billion years ago set the initial core and mantle compositions (Rubie et al., 2015), dictating their melting/freezing properties and phase relationships. The composition-dependent conditions in planetary cores that lead to the creation of solids are particularly important for the maintenance of global magnetic fields because freezing releases latent heat while partitioning of lighter elements into the liquid phase releases gravitational energy (Nimmo, 2015; Breuer and Moore, 2015). In Earth's core, the focus of this work, the release of light elements due to the ongoing growth of the solid inner core is the main power source for the present magnetic field (Braginsky, 1963), while additional power could also come from precipitation of solid phases such as MgO (O'Rourke and Stevenson, 2016; Badro et al., 2016) or SiO_2 (Hirose et al., 2017) near the top of the core. Long-term exchange of elements between the core and a solid (Buffett and Seagle, 2010; Davies et al., 2018) or liquid (Labrosse et al., 2007; Brodholt and Badro, 2017) mantle could create a stably stratified layer below the core-mantle boundary (CMB), which suppresses radial motion and enables distinct classes of wave motions (Braginsky, 1993; Buffett, 2014).

Mass exchange between Earth's core and mantle depends on the nature of the light elements and the physical conditions at the CMB. In this paper we focus on oxygen, transferred as FeO (Frost et al., 2010; Pozzo et al., 2019), which is of particular interest for

* Corresponding author.
E-mail address: c.davies@leeds.ac.uk (C.J. Davies).

https://doi.org/10.1016/j.epsl.2020.116208

several reasons. First, oxygen partitions strongly into liquid iron at the high pressures near Earth's centre (Alfè et al., 2002; Badro et al., 2014) and is therefore the prime candidate to explain the seismically-determined density drop between the solid inner core and liquid outer core (Masters and Gubbins, 2003), which cannot be accounted for by a phase change alone. Second, debate surrounding the possible precipitation of oxides below the CMB and their role in magnetic field generation (O'Rourke and Stevenson, 2016; Badro et al., 2016; Hirose et al., 2017; Du et al., 2017; Badro et al., 2018) rests heavily on the abundance of oxygen near the top of the core. Third, the presence of oxygen appears to be important for explaining a stratified layer characterised by low velocity (Helffrich and Kaneshima, 2010) and low density at the top of the core (Brodholt and Badro, 2017).

The standard model of Earth's long-term evolution assumes that the mantle froze from the bottom up during planetary differentiation (Rubie et al., 2015). In this case, little O is transferred across the CMB because mass transfer is limited by diffusion through the lower mantle chemical boundary layer, which is negligibly small in a solid (Davies et al., 2018). However, it is possible that the lower mantle did not completely solidify until much later in Earth's evolution, allowing faster mass transfer (Brodholt and Badro, 2017). This scenario is supported by the high power requirements determined by core evolution models for sustaining the geomagnetic field over the last 3.5 Gyrs (Nimmo, 2015; Davies, 2015). With high values of the thermal conductivity (de Koker et al., 2012; Pozzo et al., 2012; Gomi et al., 2013), core evolution models yield temperatures at 3.5 Ga of at least 4500 K and generally above 5000 K (Davies et al., 2015), which is far above estimates of $3500-4200$ K for the lower mantle solidus (Labrosse et al., 2015). These models predict supersolidus temperatures until the last 0.5-1.0 Ga (Nimmo, 2015; Davies et al., 2015). Evolution models based on low thermal conductivity values (Konôpková et al., 2016; Xu et al., 2018) or models that incorporate precipitation of MgO or SiO_2 at the top of the core still predict supersolidus temperatures for the first ∼1-3 Gyr (Nimmo et al., 2004; O'Rourke et al., 2017) after core formation. All of these models predict that the inner core formed less than ∼1.5 Gyrs ago: therefore FeO exchange between a fully molten core and a partially molten lower mantle may have occurred over a significant fraction of Earth's history.

Partitioning of FeO between liquid iron and a silicate Fe-O-Si liquid at pressures of 125 GPa and temperature $T = 5000-6000$ K has recently been investigated by Pozzo et al. (2019) using molecular dynamics simulations. Pozzo et al. (2019) found that oxygen partitions into liquid iron and obtained partition coefficients $P = \tilde{c}^c_O/\tilde{c}^m_{Fe} = 11.2$ at 5000 K reducing to $P = 6.6$ at 6000 K. Here $\tilde{c}^c_O$ and $\tilde{c}^m_{Fe}$ are respectively the molar concentrations of oxygen in liquid metal and iron in the silicate. These values are slightly higher than those reported in Fischer et al. (2015) and Chidester et al. (2017) at similar temperatures and lower pressures, but are consistent with the available high-temperature experimental data based on the scatter in the dataset observed at lower T. Additionally, Pozzo et al. (2019) found that the chemical reaction is exothermic and hence reduces the CMB heat flow that drives core convection.

In this work we will use the range of P values obtained by high pressure-temperature calculations (Pozzo et al., 2019) and experiments (Fischer et al., 2015) to study the long-term partitioning of oxygen into Earth's core from a partially molten magma ocean. Buffett and Seagle (2010) used the data of Frost et al. (2010) for partitioning of FeO between liquid iron and ferropericlase to model the evolution of a chemically stable layer at the top of the core subject to an imposed concentration at the CMB. Here, like Buffett and Seagle (2010), we consider a layer enriched in oxygen at the top of the core that grows downwards by diffusion. Additionally, we calculate the time-evolution of FeO concentration in the chemical boundary layer at the base of the molten mantle, which is coupled to the chemical evolution of the core through P.

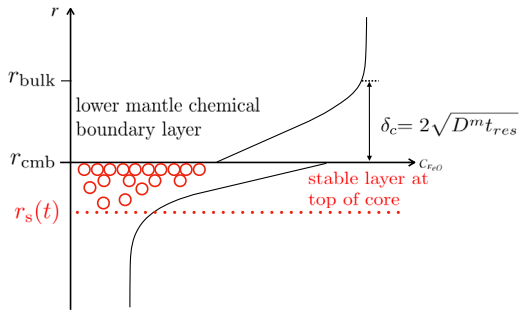

Fig. 1. Illustration of the model setup in this paper. The chemical boundary layer at the base of the magma ocean is situated directly above the CMB, radius $r_{\rm cmb}$, and is of thickness $r_{\rm bulk} - r_{\rm cmb} = \delta_c = 2\sqrt{D^m t_{res}}$ where D^m is the mass diffusion coefficient and t_{res} is the time that a fluid parcel enriched in FeO spends in direct contact with the CMB. Flux of FeO from the magma ocean enriches the top of the core in FeO, creating a stably stratified region of thickness $r_{\rm cmb} - r_s$ that grows with time t. Here r_s is the base of the layer shown by a dashed red line. Schematic profiles of the FeO concentration through both boundary layers are shown by black lines. The molar concentration of FeO on the core and magma ocean sides of the CMB are related by the partition coefficient $P = \frac{\tilde{c}^c_{FeO}(r_{\rm cmb})}{\tilde{c}^m_{FeO}(r_{\rm cmb})} = \frac{\tilde{c}^c_O(r_{\rm cmb})}{\tilde{c}^m_{Fe}(r_{\rm cmb})}$. The core and magma ocean FeO concentrations far from the CMB are assumed to be well-mixed. (For interpretation of the colours in the figure(s), the reader is referred to the web version of this article.)

We use a simple model to represent the chemical boundary layer at the base of the mantle by its thickness, the FeO concentration at the CMB as determined from P, and the bulk FeO composition of the magma ocean, which is modelled in two different ways. First, we consider an idealised scenario where the magma ocean is well-mixed with a bulk FeO concentration that does not depend on time, which allows us to focus on the evolution of the core. Solutions are computed over the 4 Gyr following core formation, which effectively assumes that the magma ocean does not freeze, for example if the temperature at the top of the core exceeded the lower mantle solidus over this time period. As such we refer to this as the "No Crystallisation" (NC) scenario. Second, Middle-Out Crystallization (MOC) models consider crystallization of the primitive mantle from the middle outwards. In this case the surface magma ocean rapidly solidifies, while the basal magma ocean (BMO) above the CMB can potentially survive until the present day (Labrosse et al., 2007). The evolution of the temperature and bulk FeO concentration as the BMO shrinks is determined by solving coupled equations determining conservation of energy and mass.

This paper is organised as follows. In section 2 we describe our model of coupled core-mantle FeO evolution. We determine the time-dependent FeO concentration at the top of the core and base of the magma ocean, the properties of the stable layer at the CMB, and the heat that is released by the exothermic reaction. The variation of these outputs as a function of model input parameters is discussed in section 3. Discussion is presented in section 4 and conclusions in section 5.

2. Methods

The model describing the simultaneous evolution of the core and magma ocean (MO) is shown schematically in Fig. 1. It is assumed that rapid convective fluctuations have been averaged out such that the equations describe the slow compositional evolution of the system (an analogous approach is used in thermal evolution models, see Gubbins et al., 2003; Nimmo, 2015). As such, all quantities are represented as functions of radius r and time t; lateral variations in composition are assumed to average out. The core and MO are assumed to be mixtures of Fe-Si-O and SiO_2-MgO-FeO

Table 1
List of parameters used in the calculations. The upper section lists parameters used in both NC and MOC models, while the lower section lists parameters that are only required to calculate the compositional evolution of the magma ocean (MO) in MOC models and are all taken from Labrosse et al. (2007). Superscripts in column 4 denote the source used for the quoted parameter values: a = Pozzo et al. (2019); b = Pozzo et al. (2013); c = Dziewonski and Anderson (1981); d = Davies et al. (2015); e = Gubbins et al. (2003).

Name	Units	Value	Reference
$\bar{c}^c_O$	–	0.05,0.13	Initial mole fraction of O (core)
$\bar{c}^c_{Si}$	–	0.08	Initial mole fraction of Si (core)
$\bar{c}^m_{FeO}$	–	0.02-0.2	Initial mole fraction of FeO (MO)
P	–	1-10	Partition coefficient^a
D^c	$m^2 s^{-1}$	5×10^{-9}	Core O diffusivity^b
D^m	$m^2 s^{-1}$	$1 \times 10^{-9} - D^c$	MO O diffusivity
ρ^c	kg m^{-3}	9900	Core density^c
ρ^m	kg m^{-3}	5500	MO density^c
t_{res}	yrs	$O(10^2 - 10^3)$	Time FeO-enriched material remains at the CMB
$\langle R_{FeO} \rangle$	ev $f.u^{-1}$	-2.5	Heat of reaction coefficient^a
dT/dr	K km^{-1}	0.1-1	Superadiabatic gradient^d
α_T	K^{-1}	10^{-5}	Core thermal expansion coefficient^e
α_c		1.1	Core O expansion coefficient^d
k	W m^{-1} K^{-1}	8	Thermal conductivity
δ_T	km	100	Upper thermal boundary layer thickness
C^b	J kg^{-1} K^{-1}	1000	MO specific heat capacity
C^c	J kg^{-1} K^{-1}	860	Core specific heat capacity
ΔS	J kg^{-1} K^{-1}	300	Entropy change on freezing
ΔT_L	K	-2000	Liquidus depression due to FeO enrichment

respectively. We restrict attention to exchange of FeO; adding MgO and SiO_2 to the model we develop is straightforward, but is not warranted at this stage. To obtain a self-consistent description of FeO exchange requires two boundary conditions at the CMB, radius $r_{\rm cmb}$, one on the FeO concentration and another on the FeO mass flux i_{FeO}. Assuming that the CMB does not move with time together with the fact that there are no point sources of mass (Loper and Roberts, 1980) requires

$$i^c_{FeO}(r_{\rm cmb}) = i^m_{FeO}(r_{\rm cmb}), \tag{1}$$

where superscripts c and m denote quantities evaluated on the core and mantle sides of the CMB respectively.

In contrast to the flux, the FeO concentration at the CMB does not have to be continuous. At chemical equilibrium the molar concentrations of FeO on each side of the CMB (denoted by overbars to distinguish from mass fractions) are determined by the partition coefficient P as

$$P = \frac{\bar{c}^c_{FeO}(r_{\rm cmb})}{\bar{c}^m_{FeO}(r_{\rm cmb})} = \frac{\bar{c}^c_O(r_{\rm cmb})}{\bar{c}^m_{Fe}(r_{\rm cmb})}. \tag{2}$$

Here the second equality arises because the concentration of FeO in the core is entirely determined by the amount of oxygen, while in the MO it is determined by the amount of Fe.

To define a well-posed problem we assume that the core sets $\bar{c}^c_{FeO}(r_{\rm cmb})$ while the MO sets i_{FeO}. The flux is then proportional to the FeO gradient in the MO, which itself depends on the variation of $\bar{c}^m_{FeO}$ across the chemical boundary layer at the base of the MO. The FeO concentration at the base of the MO, $\bar{c}^m_{FeO}(r_{\rm cmb})$, is set by $\bar{c}^c_{FeO}(r_{\rm cmb})$ through equation (2), while the FeO concentration at the top of the chemical boundary layer, radius $r_{\rm bulk}$, which we take to be the bulk FeO composition of the MO $\bar{c}^m_{FeO}(r_{\rm bulk})$, is set by the thermal evolution of the MO. In NC models $\bar{c}^m_{FeO}(r_{\rm bulk})$ is fixed in time and so i_{FeO} can be calculated from the evolution of $\bar{c}^c_{FeO}(r_{\rm cmb})$ as described in section 2.1 below. In MOC models $\bar{c}^m_{FeO}(r_{\rm bulk})$ varies as the BMO evolves in time. This calculation is described in section 2.2. These feedbacks mean that the boundary conditions given by equation (1) and (2) vary with time.

FeO dissolution is accompanied by heat release at the CMB, which affects the core energy budget and the operation of the geodynamo. The reaction is exothermic because the heat of reaction coefficient is negative, $\langle R_{FeO} \rangle = R^c_{FeO} - R^m_{FeO} < 0$, in contrast to the positive values of $\langle R_{FeO} \rangle$ that arise for FeO partitioning between liquid metal and ferropericlase (Davies et al., 2018). Here $R_{FeO} = \mu - T(\partial \mu / \partial T)_{P,T}$, where μ is the chemical potential, and we use the value $\langle R_{FeO} \rangle = -2.5$ ev per formula unit of FeO as obtained by Pozzo et al. (2019). The reaction does not directly alter the power available to the geodynamo because heat input and output occur at the same radius, but does so indirectly by changing the CMB heat flow. In the Appendix we show that the heat $Q_{\rm m}$ extracted across the lower mantle thermal boundary layer is related to the heat $Q_{\rm c}$ driving core convection by $Q_{\rm c} = Q_{\rm m} + Q_{\rm h} = Q_{\rm m} + 4\pi r^2_{\rm cmb} \langle R_{FeO} \rangle |i_{FeO}|$. Since $\langle R_{FeO} \rangle < 0$, $Q_{\rm h} < 0$ and the reaction decreases $Q_{\rm c}$ for a given $Q_{\rm m}$, which in turn lowers the core cooling rate and decreases the power available to the geodynamo (Nimmo, 2015). Evaluating $Q_{\rm h}$ is straightforward once the FeO flux is determined.

2.1. NC models: FeO evolution at the top of the core

The mass fraction of O in the core, c^c_O, satisfies the differential equation

$$\frac{\partial c^c_O}{\partial t} = D^c \nabla^2 c^c_O = \frac{D^c}{r^2} \frac{\partial}{\partial r} \left(r^2 \frac{\partial c^c_O}{\partial r} \right), \tag{3}$$

subject to the CMB boundary condition given by Fick's law of mass diffusion:

$$\left. \frac{\partial c^c_O}{\partial r} \right|_{r_{\rm cmb}} = -\frac{i_O}{\rho^c D^c}. \tag{4}$$

Here r is radius, $i_O = i_{FeO} A_O / A_{FeO}$ is the normal component of the mass flux of oxygen (defined negative when the flux is into the core), $A_{FeO} = A_O + A_{Fe}$, and D^c is the mass diffusion coefficient of O in liquid iron (parameters and their values are listed in Table 1). The atomic weights of oxygen, A_O, and iron, A_{Fe}, convert the FeO flux into an O flux. Equation (4) omits the barodiffusive contribution to i_O (Gubbins and Davies, 2013), which we expect to be small in comparison to the FeO flux from the MO. This is verified by our results.

We assume that i_O is determined by diffusion in the MO overlying the core. Even if the magma ocean convects vigorously

(Labrosse et al., 2007, 2015), chemical exchange is still accomplished by diffusion through a thin boundary layer since the large density jump at the CMB significantly hinders vertical motion. It is possible that rapid instability of the chemical boundary layer could control i_O; however, this mechanism relies on poorly known quantities such as the lengthscale of the instability and viscosity contrast between depleted and enriched layers (Ribe, 1998). In practice the strength of both mechanisms is related to the time t_{res} that a fluid parcel enriched in FeO spends in direct contact with the CMB, which we vary within reasonable limits. Assuming that the FeO gradient in the chemical boundary layer at the base of the MO can be approximated by a linear variation, the FeO flux into the core can be written

$$i^m_{FeO} = -\rho^m D^m \frac{\partial c^m_{FeO}}{\partial r} \approx \rho^m D^m \frac{c^m_{FeO}(r_{\rm cmb}) - c^m_{FeO}(r_{\rm bulk})}{\delta_c}, \tag{5}$$

where δ_c is the thickness of the chemical boundary layer at the base of the MO. Equations (1), (4) and (5) imply that

$$\left.\frac{\partial c^c_O}{\partial r}\right|_{r_{\rm cmb}} = -\frac{i^m_{FeO}}{\rho^c D^c}\frac{A_O}{A_{FeO}} \approx \frac{\rho^m D^m}{\rho^c D^c}\frac{c^m_{FeO}(r_{\rm cmb}) - c^m_{FeO}(r_{\rm bulk})}{\delta_c}. \tag{6}$$

Equation (6) is used to evaluate $\partial c^c_O/\partial r$ in terms of δ_c, $c^m_{FeO}(r_{\rm cmb})$ and $c^m_{FeO}(r_{\rm bulk})$. The chemical boundary layer thickness is estimated as $\delta_c = r_{\rm bulk} - r_{\rm cmb} \approx 2\sqrt{D^m t_{res}}$, where D^m is the mass diffusion coefficient. The mass fraction of FeO at the base of the MO, $c^m_{FeO}(r_{cmb})$, is determined from equation (2) using the value of P. To relate mole fractions, which arise in the definition of P and are denoted by overbars, to the mass fractions that are used in equations (3) and (6) we use

$$c^c_O = \frac{\bar{c}^c_O A_O}{(\bar{c}^c_O A_O + \bar{c}^c_{Si} A_{Si} + (1 - \bar{c}^c_O - \bar{c}^c_{Si})A_{Fe})} \tag{7}$$

in the core and

$$c^m_{FeO} = \frac{\bar{c}^m_{FeO} A_{FeO}}{(\bar{c}^m_{FeO} A_{FeO} + \bar{c}^m_{SiO_2} A_{SiO_2} + A_{MgO}\bar{c}^m_{MgO})} \tag{8}$$

in the MO. Here $A_{MgO} = A_O + A_{Mg}$ and $A_{SiO_2} = A_{Si} + 2A_O$. Since we are focusing on FeO exchange the molar fractions of SiO_2, $\bar{c}^m_{SiO_2}$, and MgO, $\bar{c}^m_{MgO}$, do not change through partitioning but are instead set such that $\bar{c}^m_{SiO_2} = (1-x)(1-\bar{c}^m_{FeO})$ and $\bar{c}^m_{MgO} = x(1-\bar{c}^m_{FeO})$, where x determines the fractions of $\bar{c}^m_{SiO_2}$ and $\bar{c}^m_{MgO}$. The mass fractions obtained from equation (8) using the end-member values $x = 0$ and $x = 1$ differ by at most a factor of 1.5, which arises when $\bar{c}^m_{FeO} = 0$. However, the value of x is actually unimportant since it is the FeO concentration difference between the CMB and bulk MO rather than the individual concentrations that are relevant for evaluating the model equations (see equation (6)). We therefore choose $x = 1$ without any loss of generality.

2.2. MOC models: determination of the bulk magma ocean concentration

In NC models the bulk MO FeO concentration $c^m_{FeO}(r_{\rm bulk})$ in equation (6) is assumed to retain a constant value in time. In MOC models it is determined by the global energy and mass balances governing the slow evolution of the MO. For this calculation the basic setup and all parameter values are taken from Labrosse et al. (2007). Here we generalise the mass balance used in Labrosse et al. (2007) to account for loss of FeO from the MO to the core, which affects the growth and cooling rate of the magma ocean.

The global energy equation balances the heat $Q_{\rm bmo}$ extracted from the BMO against the secular cooling $Q_{\rm s}$, radiogenic heating $Q_{\rm r}$, latent heat $Q_{\rm L}$ released on freezing, and the heat $Q_{\rm m}$ entering the BMO from below and can be written (Labrosse et al., 2007)

$$\underbrace{4\pi a^2 k \frac{T_L - T_M}{\delta_T}}_{Q_{\rm bmo}} = \underbrace{-M^m C^m \frac{{\rm d}T_L}{{\rm d}t}}_{Q_{\rm s}} \underbrace{-M^c C^c \frac{{\rm d}T_L}{{\rm d}t}}_{Q_{\rm m}} + \underbrace{H(t)}_{Q_{\rm r}} \underbrace{-4\pi a^2 \rho^m \Delta S T_L \frac{{\rm d}a}{{\rm d}t}}_{Q_{\rm L}}, \tag{9}$$

where a is the upper radius of the BMO, T_L is the BMO liquidus temperature, T_M is the temperature of the solid mantle (assumed constant), k is the BMO thermal conductivity, δ_T is the thickness of the thermal boundary layer at the top of the BMO (assumed constant), C^m and C^c are the BMO and core specific heat capacities and $M^m = 4\pi\rho^m(a^3 - r^3_{\rm cmb})/3$ and M^c their respective masses. $H(t)$ is the rate of radiogenic heat production and ΔS is the entropy change on freezing. Equation (9) is solved for the cooling rate ${\rm d}T_L/{\rm d}t$ by relating it to the freezing rate of the MO, ${\rm d}a/{\rm d}t$.

Equation (9) presents a somewhat simplified view of thermal coupling between the core and MO because the form of $Q_{\rm m}$ assumes that the cooling rates of the core and BMO are equal (to ${\rm d}T_L/{\rm d}t$) and independent of radius. In actual fact $Q_{\rm m}$ is determined by the properties of the thermal boundary layer at the base of the MO, usually in the same fashion as the estimate of $Q_{\rm bmo}$ in equation (9) and i_{FeO} in section 2.1, and so the cooling rates vary with depth. The assumed form of $Q_{\rm m}$ in equation (9) allows the evolution of the MO to be determined without calculating the thermal evolution of the core. However, this presents a problem when accounting for the heat $Q_{\rm h}$ released by the exothermic reaction because $Q_{\rm h}$ does not appear directly in the global energy balance; instead, its effect is to change the core cooling rate and hence the core temperature. This can be seen by noting that, prior to inner core formation, $Q_{\rm m} = Q_{\rm c} - Q_{\rm h} = \int \rho C^c ({\rm d}T/{\rm d}t){\rm d}V^c$, where V^c is the core volume. The core cooling rate ${\rm d}T/{\rm d}t$ must equal the BMO cooling rate at the CMB (for continuity of temperature) but will not generally equal the cooling rate of the bulk BMO. The resolution to this apparent contradiction is that the core must respond to an imposed $Q_{\rm m}$ by changing the CMB temperature, which acts to modify $Q_{\rm m}$, thus requiring a calculation of the coupled thermal evolution of core and mantle (viz Nimmo et al., 2004; Nakagawa and Tackley, 2014; Driscoll and Bercovici, 2014). Nevertheless, despite the simplified form of equation (9) we continue to use it as this enables the effect of FeO transfer to the core to be understood within the context of an established model.

To relate ${\rm d}T_L/{\rm d}t$ and ${\rm d}a/{\rm d}t$ we begin with mass conservation of FeO, which can be written

$$\frac{{\rm d}\left(c^m_{FeO}M^m + c^s_{FeO}M^s + c^c_{FeO}M^c\right)}{{\rm d}t} = 0, \tag{10}$$

where M^s and c^s_{FeO} are the mass and FeO mass fraction of the solid mantle. Noting that the total mass $M^{tot} = M^m(t) + M^s(t) + M^c(t)$ is independent of time, equation (10) becomes

$$M^m \frac{{\rm d}c^m_{FeO}}{{\rm d}t} = \Delta c \frac{{\rm d}M^s}{{\rm d}t} + c^m_{FeO}\frac{{\rm d}M^c}{{\rm d}t} - M^s\frac{{\rm d}c^s_{FeO}}{{\rm d}t} - \frac{{\rm d}(c^c_{FeO}M^c)}{{\rm d}t}, \tag{11}$$

where $\Delta c = c^m_{FeO} - c^s_{FeO}$ is the enrichment of melt in FeO relative to the solid. Following Labrosse et al. (2007) we neglect the term $M^s({\rm d}c^s_{FeO}/{\rm d}t)$, which is appropriate since concentration variations in the solid mantle are expected to be slow (Davies et al., 2018), and write ${\rm d}M^s/{\rm d}t = -4\pi a^2 \rho^s {\rm d}a/{\rm d}t$, which assumes that changes in the solid mantle arise solely from growth of the BMO. With these approximations and assuming $\rho^s = \rho^m$ we obtain

$$\frac{\mathrm{d}c^m_{FeO}}{\mathrm{d}t} = -\frac{3a^2\Delta c}{(a^3 - r^3_{\mathrm{cmb}})}\frac{\mathrm{d}a}{\mathrm{d}t} + \frac{c^m_{FeO}}{M^m}\frac{\mathrm{d}M^c}{\mathrm{d}t} - \frac{1}{M^m}\frac{\mathrm{d}(c^c_{FeO}M^c)}{\mathrm{d}t}. \quad (12)$$

The first two terms in equation (12) describe the mass balance used by Labrosse et al. (2007), while the final two terms on the right-hand side represent the effect of mass exchange with the core. To estimate the third term we note that the total core mass and the total core FeO mass, M^c_{FeO}, can be written respectively as $M^c = A_{FeO}N_{FeO} + A_{Fe}N_{Fe} + A_{Si}N_{Si}$ and $M^c_{FeO} = A_{FeO}N_{FeO}$, where N_X denotes the number of atoms of element X. In our model M^c changes only through the addition of FeO, in which case $\mathrm{d}N_{Fe}/\mathrm{d}t = \mathrm{d}N_{Si}/\mathrm{d}t = 0$ and therefore $\mathrm{d}M^c/\mathrm{d}t = \mathrm{d}(c^c_{FeO}M^c)/\mathrm{d}t$. The last two terms in equation (12) can then be combined into the term $-((1 - c^m_{FeO})/M^m)(\mathrm{d}(c^c_{FeO}M^c)/\mathrm{d}t)$, which can be calculated from the equation for conservation of FeO between the core and MO,

$$\frac{\mathrm{d}}{\mathrm{d}t}\left(\int \rho c^c_{FeO}\,\mathrm{d}V\right) = \frac{\mathrm{d}\left(c^c_{FeO}M^c\right)}{\mathrm{d}t} = -4\pi r^2_{\mathrm{cmb}} i_{FeO} = -I_{FeO}. \quad (13)$$

Here we have assumed that $c^c_{FeO}(r)$ does not vary across the core, which we find a posteriori to be a good approximation because the region where c^c_{FeO} varies is thin compared to the core. The final mass balance is then

$$\frac{\mathrm{d}c^m_{FeO}}{\mathrm{d}t} = -\frac{3a^2\Delta c}{(a^3 - r^3_{\mathrm{cmb}})}\frac{\mathrm{d}a}{\mathrm{d}t} + \frac{3r^2_{\mathrm{cmb}}(1 - c^m_{FeO})i_{FeO}}{\rho^m(a^3 - r^3_{\mathrm{cmb}})}, \quad (14)$$

which shows that the FeO concentration of the MO increases as the magma ocean freezes and decreases as FeO is lost to the core (i.e. if $i_{FeO} < 0$).

The MO is assumed to be at the liquidus temperature. Though more complex phase relations exist (e.g. Boukaré et al., 2015) we consider the simple liquidus relation used by Labrosse et al. (2007), $\mathrm{d}c^m_{FeO}/\mathrm{d}t = (\Delta c_L/\Delta T_L)\mathrm{d}T_L/\mathrm{d}t$ where $\Delta T_L = -2000$ K is the drop in the liquidus temperature that arises as the FeO concentration increases from zero to one ($\Delta c_L = 1$). This equation allows the freezing rate of the MO to be written

$$\frac{\mathrm{d}a}{\mathrm{d}t} = -\frac{(a^3 - r^3_{\mathrm{cmb}})}{3a^2\Delta c\Delta T_L}\frac{\mathrm{d}T_L}{\mathrm{d}t} + \frac{r^2_{\mathrm{cmb}}(1 - c^m_{FeO})i_{FeO}}{\rho^m a^2\Delta c}. \quad (15)$$

The first term on the right-hand side of equation (15) shows that the MO shrinks as it cools. The second term shows that FeO transfer to the core can increase the freezing rate of the MO. This can be understood by setting $\mathrm{d}c^m_{FeO}/\mathrm{d}t = 0$ (and hence $\mathrm{d}T_L/\mathrm{d}t = 0$), in which case maintaining the same mass fraction of FeO while losing FeO to the core requires the magma ocean to shrink. However, FeO loss to the core slows down enrichment of the BMO in FeO, which in turn slows down the cooling rate through the liquidus relation.

Using equation (15) the latent heat term in equation (9) now becomes

$$Q_{\mathrm{L}} = \frac{4\pi\rho^m\Delta S T_L(a^3 - r^3_{\mathrm{cmb}})}{3\Delta c\Delta T_L}\frac{\mathrm{d}T_L}{\mathrm{d}t} - \frac{4\pi r^2_{\mathrm{cmb}}(1 - c^m_{FeO})i_{FeO}T_L\Delta S}{\Delta c},$$
$$= Q^c_{\mathrm{L}} + Q^{FeO}_{\mathrm{L}}.$$

The cooling rate can then be obtained from equation (9):

$$\frac{\mathrm{d}T_L}{\mathrm{d}t} = \frac{Q_{\mathrm{bmo}} - Q_{\mathrm{R}} + 4\pi r^2_{\mathrm{cmb}}(1 - c^m_{FeO})i_{FeO}T_L\Delta S/\Delta c}{(-M^c C^m - M^s C^c + \tilde{Q}^c_{\mathrm{L}})}, \quad (16)$$

where $Q^c_{\mathrm{L}} = \tilde{Q}^c_{\mathrm{L}}\mathrm{d}T_L/\mathrm{d}t$. The term $4\pi r^2_{\mathrm{cmb}}(1 - c^m_{FeO})i_{FeO}T_L\Delta S/\Delta c$ that arises from FeO loss to the core acts with the radiogenic heating to offset heat loss out of the BMO (Q_{bmo}) and slow its cooling.

2.3. Implementation and parameter values

Equation (3) and the boundary conditions are numerically integrated forward in time for 4 billion years starting 4.5 billion years before present. The most recent 0.5 Gyrs are omitted to avoid complicating factors due to the formation and growth of the inner core (Buffett and Seagle, 2010; Nimmo, 2015; Davies, 2015). At each step $\bar{c}^c_O(r_{cmb})$ is used to determine $\bar{c}^m_{Fe}(r_{cmb})$ from P. Together with $\bar{c}^m_{Fe}(r_{bulk})$ this sets i_O from equation (6), which provides the updated boundary condition on equation (3) and the process repeats. For practical reasons equation (3) is solved in a fixed 400 km-thick domain at the top of the core, which is much thicker than the stable regions that grow in any of our calculations. A zero flux condition is prescribed at $r = 3080$ km. Entrainment may erode the base of the layer, but we expect the inward flux of light element at the CMB to exceed the outward flux at the base of the layer (Buffett and Seagle, 2010; Gubbins and Davies, 2013) and therefore set the latter to zero for simplicity.

Parameter values used for both NC and MOC models are listed in the top section of Table 1. The core is assumed to be initially well-mixed with $\bar{c}^c_{Si} = 0.08$ (Davies et al., 2015) and $\bar{c}^c_O = 0.05$ or 0.13, which are chosen in order that the final values from the model are close to matching values of $\bar{c}^c_O = 0.08 - 0.17$ estimated for Earth's present day core based on the ICB density jump and core mass (Hirose et al., 2013; Badro et al., 2014; Davies et al., 2015). Estimates of the initial bulk magma ocean iron content range between 10-20% (Andrault et al., 2012; Tateno et al., 2014). To assess the sensitivity of the model to this parameter we consider the wider range $\bar{c}^m_{FeO} = 2 - 20\%$.

We consider a range of P values that span the range of theoretical and experimental determinations at high pressures and temperatures. The appropriate pressure is 135 GPa, which is almost reached by the simulations of Pozzo et al. (2019); however, very few experimental studies of partitioning have been conducted above 80 GPa (see e.g. Fischer et al., 2015; Pozzo et al., 2019) Since we are interested in early CMB conditions the relevant temperature is ∼5000 K and at least 4000 K, which is the current CMB temperature (Nimmo, 2015; Davies et al., 2015). Figure 2 of Pozzo et al. (2019) combines the dataset of oxygen distribution coefficients, K_d, compiled by Fischer et al. (2015) with some more recent studies and contains 12 experimental points at temperature greater than 4000 K. All of these data have molar Fe concentrations in the liquid of ∼0.5 and hence values of P are larger than the corresponding K_d value by about a factor of 2. For these data the lowest value of K_d is 0.64, corresponding to $P = 1.24$ using the values of $\bar{c}^c_O$ in Fischer et al. (2015). The largest values are those obtained by Pozzo et al. (2019), which give $P \sim 10$. We therefore consider the range $1 \leq P \leq 10$. For illustration we take P as independent of time.

The diffusivity of oxygen in the core is taken from our previous work (Pozzo et al., 2013) and most calculations assume $D^m = D^c$. A calculation with $D^m = 5 \times 10^{-9}$ m^{2}s^{-1} and $D^c = 10^{-9}$ m^{2}s^{-1} produces values of $\bar{c}^c_O(r_{cmb})$ after 4 Gyrs that differ by less than 1%. The chemical boundary layer thickness δ_c depends on both D^m and the residence time t_{res}. Convective velocities of ∼1-10 cm yr^{-1} in the MO (Solomatov, 2015; Ziegler and Stegman, 2013) suggest that $t_{res} = O(10^{-2} - 10^2)$ yrs, but we expect radial flow to be impeded near the CMB and therefore assume a more conservative range $t_{res} = O(10^2 - 10^3)$ yrs (in the sense that higher values of t_{res} reduce i_O with all other parameters fixed). Clearly some of these input parameters are subject to significant uncertainties. Here we do not attempt an exhaustive parameter exploration, but consider a range of plausible values that demonstrate the physics of the problem. MOC models employ the parameter values in the upper and middle sections of Table 1.

The model outputs in all cases are the time-dependent core oxygen concentration, CMB FeO flux, heat Q_{h} released at the CMB

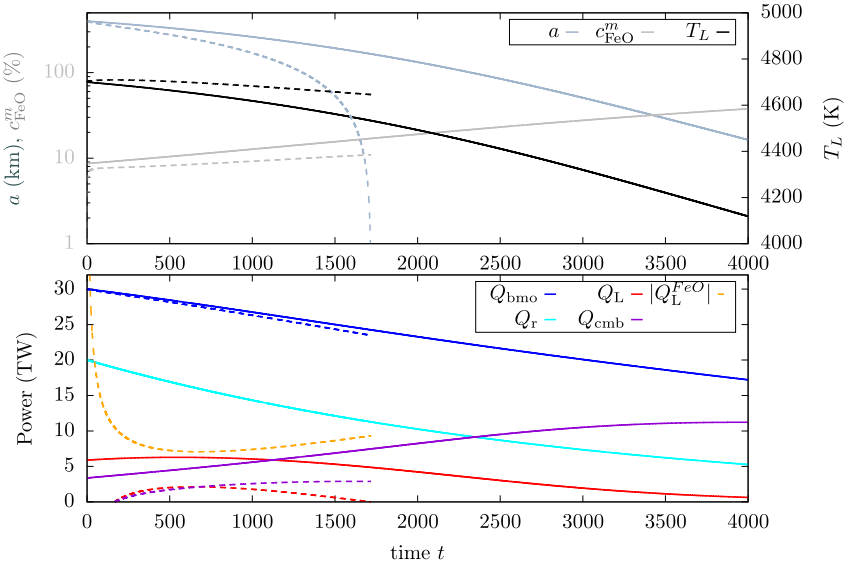

Fig. 2. Example calculation showing the evolution of the basal magma ocean (BMO) using $P = 10$ and initial uniform concentrations $\bar{c}^m_{FeO} = 0.05$ and $\bar{c}^c_O = 0.05$. Top shows BMO temperature (right ordinate), BMO radius (left ordinate, blue-grey) and $\bar{c}^m_{FeO}$ (left ordinate, light grey). Bottom shows contributions to the BMO energy budget: the heat leaving the BMO $Q_{\rm bmo}$, radiogenic heating $Q_{\rm r}$, CMB heat flow $Q_{\rm cmb}$, latent heat released due to growth of the BMO $Q^c_{\rm L}$, and FeO loss to the core $Q^{FeO}_{\rm L}$. Solid (dashed) lines show BMO evolution without (with) FeO loss to the core.

due to the exothermic reaction and the thickness of the chemically stable layer at the top of the core. In MOC models we additionally calculate the time-dependence of T_L, a and the individual terms in the energy balance. The base of the chemically stable layer is calculated by comparing the stabilising compositional gradient, obtained as a solution of equation (3), to the destabilising gradients. We set the destabilising gradient equal to $\alpha_T/\alpha_c {\rm d}T/{\rm d}r$ where ${\rm d}T/{\rm d}r$ is the superadiabatic gradient and α_c and α_T are the compositional and thermal expansion coefficients given in Table 1. The variation in ${\rm d}T/{\rm d}r$ changes the estimated layer thickness by only a few kilometres.

3. Results

We first demonstrate the influence of FeO loss to the core on the evolution of the BMO before comparing NC and MOC cases. Fig. 2 shows an example MOC model evolution both with and without the effect of FeO transfer to the core. Without FeO loss, the MO evolution is as shown in Labrosse et al. (2007). The addition of FeO loss slows FeO enrichment of the BMO and reduces the cooling rate as required to keep the BMO on the liquidus. The rate at which the BMO shrinks is determined by the competition between cooling and FeO loss (second and third terms in equation (15)), which can be comparable at early times depending primarily on the values of P and $\bar{c}^m_{FeO}$. However, at later times the term due to FeO loss tends to dominate, which causes the BMO to shrink faster than in Labrosse et al. (2007). The net effect is that FeO loss hastens the complete solidification of the BMO; in the example in Fig. 2 the mantle is completely solid after 1.7 Gyrs of evolution with FeO loss, while the BMO lasts until the present day in its absence.

The early stages of chemical exchange are characterised by rapid changes in the FeO flux. Fig. 3 illustrates the range of initial behaviour for NC and MOC models. In all models the top of the core becomes rapidly enriched in O, which produces a sharp reduction in the FeO flux in the first few hundred Myrs followed by a much slower compositional evolution. In NC models the total flux of FeO at the CMB, I_{FeO}, decreases monotonically over time because the bulk FeO concentration of the MO is fixed while the FeO concentration at the base of the MO steadily increases as more FeO partitions into the core. MOC models exhibit three broad regimes of behaviour following the initial rapid decline in I_{FeO}. In the 'low flux' regime, FeO enrichment due to fractional crystallization exceeds FeO loss to the core and I_{FeO} increases slowly over time, with more O partitioning into the core than in the corresponding NC model. Models in this regime have [$\bar{c}^m_{FeO} = 0.05, 0.02; 1 \le P \le 10$], [$\bar{c}^m_{FeO} = 0.1; P < 8$], [$\bar{c}^m_{FeO} = 0.15; P < 5$], and [$\bar{c}^m_{FeO} = 0.2; P < 3$]. In the 'moderate flux' regime FeO loss and gain are in approximate balance and MOC and NC models follow a similar evolution. In the 'high flux' regime, which corresponds broadly with $P = 10$ and $\bar{c}^m_{FeO} \ge 0.1$ in our suite of runs, FeO loss exceeds gain and the MO is slowly depleted. In this regime it is possible for $\bar{c}^c_O(r_{\rm cmb})$ to decline over time despite the fact that FeO flux is still into the core. This arises when a large initial CMB flux sets up a steep chemical gradient at the top of the core: flux of FeO to the deeper core down this gradient exceeds flux of FeO into the core during the subsequent evolution as the CMB gradient rapidly declines.

Fig. 4 shows the long-timescale evolution of the runs in Fig. 3. In NC models the only timescale in the problem is the diffusive timescale and so $\bar{c}^c_O(r_{\rm cmb})$ increases proportionally to $\sqrt{t}$ as expected. It then follows that i_{FeO} decreases as $1/\sqrt{t}$. The total FeO flux transferred in time t, $M^c_{FeO}(t) = \int_0^t i_{FeO}(t'){\rm d}t'$, then increases as $\sqrt{t}$ as shown in Fig. 4a. The thickness of the stable region also evolves as $\sqrt{t}$ (Fig. 4b) because the inward flux of FeO at the CMB greatly exceeds the outward flux due to entrainment at the base of the layer. The evolution of $Q_{\rm h}$ follows that of i_{FeO} (Fig. 4c).

Model behaviour is relatively insensitive to the initial core concentration and so we summarise the results in terms of P and $\bar{c}^m_{FeO}(r_{\rm bulk})$. Fig. 5 shows $\bar{c}^c_O$ at the CMB, the CMB flux of O, $I_O = I_{FeO} A_O/(A_{FeO})$, the total amount of O that entered the core, $M^c_O = M^c_{FeO} A_O/(A_{FeO})$, and the thickness of the stably stratified layer at the CMB, $r_{\rm cmb} - r_s$, all evaluated at $t = 1$ and 4 Gyrs for all NC models. All quantities increase with P and $\bar{c}^m_{FeO}(r_{\rm bulk})$. Early mass fluxes are generally $O(10^4 - 10^5)$ kg s^{-1}, but drop by only a factor of 2-3 over the subsequent 3 Gyrs (Fig. 5a). The only exceptions are models with $\bar{c}^m_{FeO} = 0.02$ and $P \le 2$, where I_O is weak and positive, i.e. into the mantle. In the first 1 Gyr models with $\bar{c}^m_{FeO} \ge 0.10$ and $P \ge 5$ evolve to a CMB composition that is at

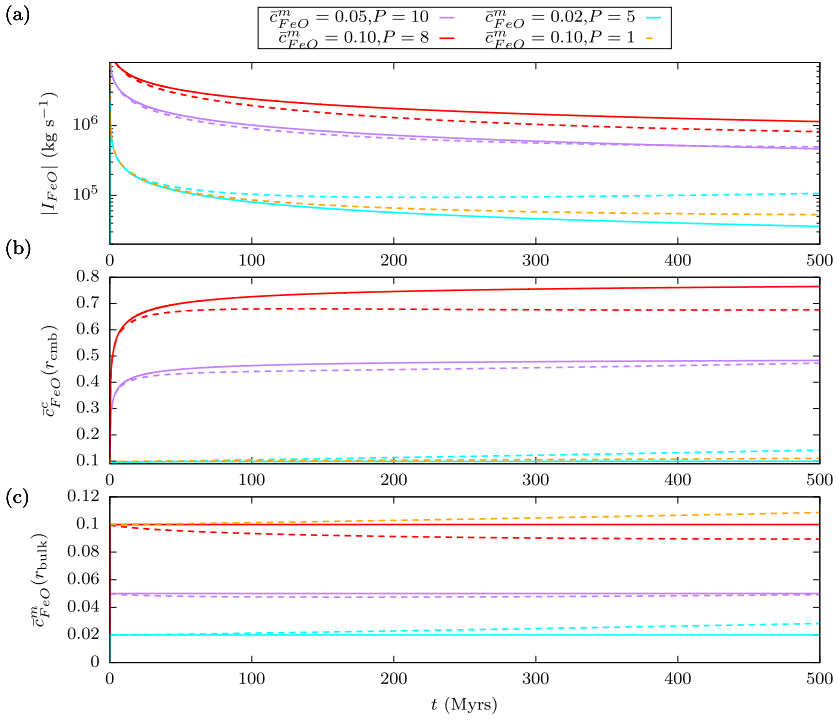

Fig. 3. Initial evolution of the core-magma ocean system. Total flux of FeO across the CMB I_{FeO} (a), and molar concentration of FeO at the top of the core (b) and in the bulk of the MO (c) as functions of time for the first 500 Myrs of evolution. NC models are shown by solid lines and MOC models are shown with dashed lines. Legend lists the initial MO concentrations; initially $\bar{c}^c_O = 0.05$ in all cases.

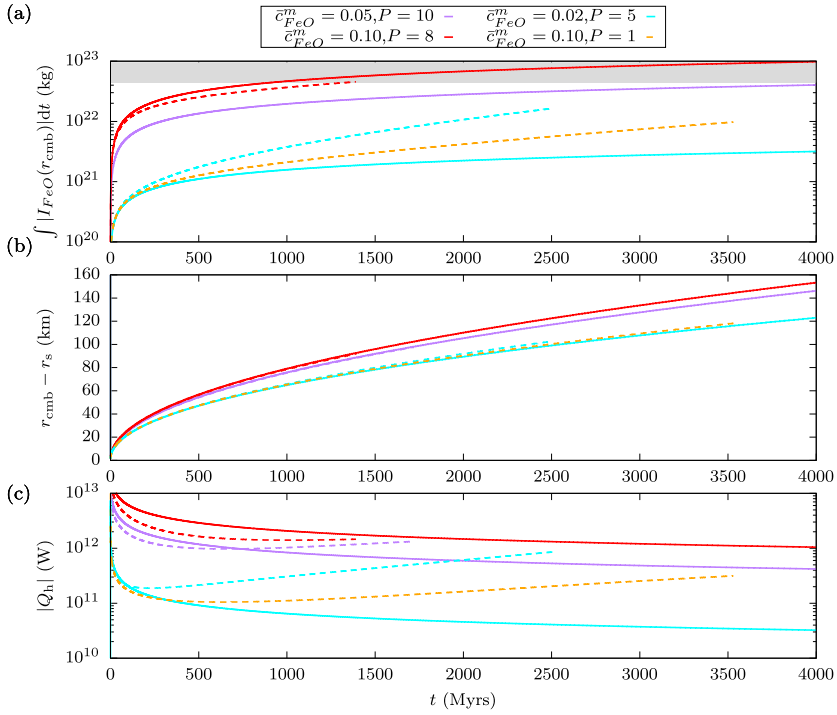

Fig. 4. Long-term evolution of the core-magma ocean system for the cases shown in Fig. 3. Time-series showing the cumulative amount of O in the core with present-day concentrations depicted by the grey band (top), thickness of the chemically stable layer that grows downwards from the CMB (middle) and the total heat released from dissolution of FeO at the CMB. NC models are shown by solid lines and MOC models are shown with dashed lines. Legend lists the initial MO concentrations; initially $\bar{c}^c_O = 0.05$ in all cases.

least 50% O (i.e. pure FeO), while the highest values lead to an uppermost core that is almost pure O (Fig. 5b).

Perhaps the most striking result concerns the total transfer of O into the core (Fig. 5c). If the MO survived for 1 Gyrs then FeO transfer across the CMB with $\bar{c}^m_{FeO} \geq 0.1$ and $P \geq 10$ could provide over a quarter of the core's present-day oxygen, while the existence of the MO for 4 Gyrs would transfer all of the present core oxygen. With $\bar{c}^m_{FeO} = 0.02$ and 0.05 mass transfer is small for all values of P. Finally, stable layer thicknesses reach 60-70 km after 1 Gyrs and double in the remaining 3 Gyrs (Fig. 5d).

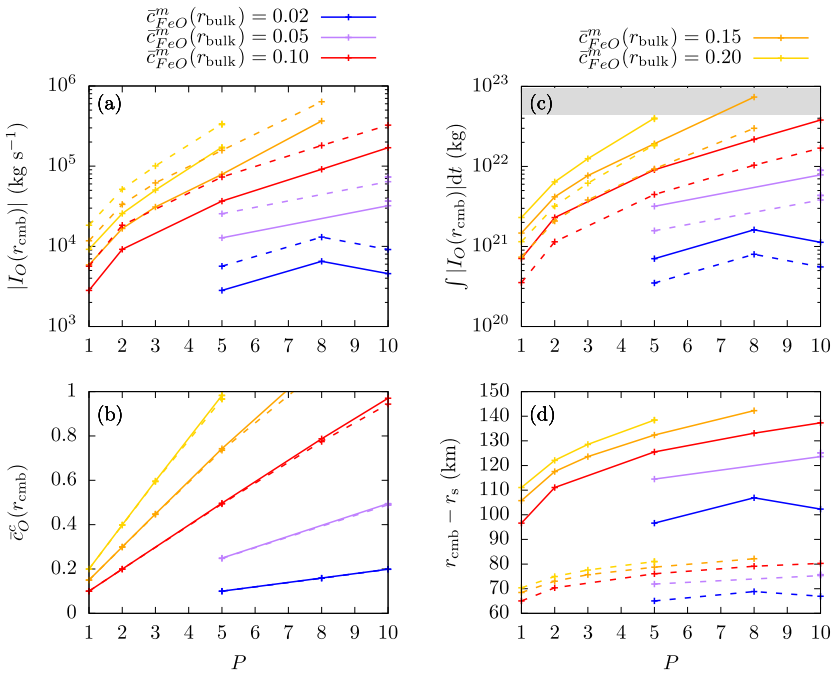

Fig. 5. Parameter study of NC models. Each panel shows results after 1 Gyr of evolution in dashed lines and 4 Gyrs in solid lines for different values of the bulk FeO concentration of the MO $\bar{c}^m_{FeO}$ and partition coefficient P. (a) magnitude of the oxygen flux into the core at the CMB, $|I_O(r_{\rm cmb})|$; (b) molar core oxygen concentration at the CMB, $\bar{c}^c_O(r_{\rm cmb})$; (c) total oxygen flux integrated from time zero to 1 Gyrs (dashed) and 4 Gyrs (solid), $\int |I_O(r_{\rm cmb})| {\rm d}t$, where the grey shaded region shows the estimated mass of O in the present-day core from Davies et al. (2015); (d) thickness of the chemically stable layer below the CMB, $r_{\rm cmb} - r_s$.

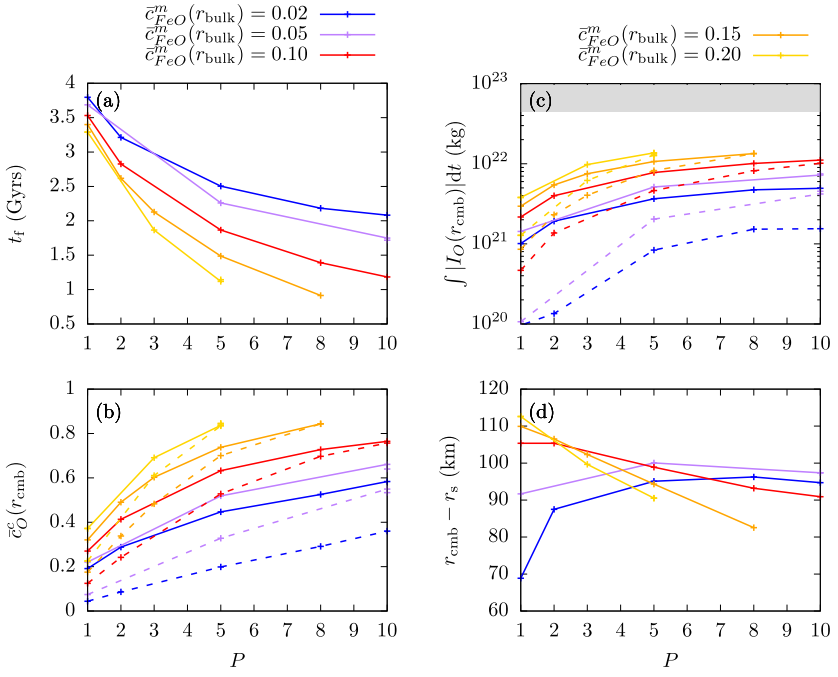

Fig. 6. Parameter study of MOC models. Each panel shows results for different initial values of the bulk FeO concentration of the MO $\bar{c}^m_{FeO}$ and partition coefficient P. Dashed lines show values calculated after 1 Gyr of evolution, while solid lines show values calculated at the time when the magma ocean completely crystallized, which is t_f Gyrs after the start of the run as shown in panel (a). (b) molar core oxygen concentration at the CMB, $\bar{c}^c_O(r_{\rm cmb})$; (c) total oxygen flux integrated from time zero to 1 Gyrs (dashed) and 4 Gyrs (solid), $\int |I_O(r_{\rm cmb})| {\rm d}t$, where the grey shaded region shows the estimated mass of O in the present-day core from Davies et al. (2015); (d) thickness of the chemically stable layer below the CMB, $r_{\rm cmb} - r_s$.

Fig. 6 summarises MOC models in terms of $\bar{c}^c_O(r_{\rm cmb})$, M^c_O, $r_{\rm cmb} - r_s$ and the time t_f taken for the magma ocean to completely crystallize. With FeO loss to the core the BMO does not survive for 4 Gyrs in any of our models; its lifetime decreases from ∼3 Gyrs for the lowest values of $\bar{c}^m_{FeO}$ and P to less than 1 Gyr for the highest values of $\bar{c}^m_{FeO}$ and P. After 1 Gyr of evolution (shown as dashed lines in Figs. 5 and 6) the 'low flux' MOC models show greater FeO transfer to the core than the corresponding NC model, while the opposite is true for the 'high flux' cases (see Fig. 4). The thickness of the chemically stable layer decreases with P because there is less time for the stabilising chemical anomalies to diffuse to greater depths.

4. Discussion

Our model makes several simplifying assumptions that are worthy of further scrutiny. First, we have only considered FeO exchange even though the magma ocean was likely rich in MgO and SiO_2. The addition of more elements is straightforward: each is governed by a diffusion equation that can be solved following the procedures used here, with coupling between the solutions arising from the partition coefficients, which will generally be functions of concentration. Additionally, transfer of each species $X \in \{\mathrm{FeO}, \mathrm{MgO}, \mathrm{SiO_2}\}$ releases or absorbs an amount of heat $Q_\mathrm{h}^X = 4\pi r_\mathrm{cmb}^2 \langle R_X \rangle |i_X|$ depending on whether the associated reaction is exothermic or endothermic and the total heat of reaction $Q_\mathrm{h} = \sum Q_\mathrm{h}^X$ could be included in the energy balance using the theory developed here for FeO. However, despite much progress (e.g. Fischer et al., 2015; Badro et al., 2018; Du et al., 2017; Pozzo et al., 2019, and references therein) the temperature- and composition-dependence of Mg and Si partitioning between iron alloys and silicate melts at CMB conditions is still debated and rather uncertain. In view of this and the fact that the addition of more elements does not change the basic physics, we believe that such complications are not warranted at present.

Our treatment of the magma ocean boundary layer is also potentially too simple because it is likely that the residence time t_{res} of material in the boundary layer will evolve as temperature and composition conditions change with time. It is also possible that the boundary layer could become unstable, which could be parameterized as in, e.g., Ribe (1998), at the expense of introducing more uncertain model inputs. Such complexities would require detailed theoretical or computational investigation that could be the topic of future study.

We have considered two scenarios for the bulk evolution of the magma ocean, which each have benefits and drawbacks. In the idealised scenario of No Crystallization the bulk magma ocean composition was assumed to be constant in time and hence the FeO flux evolves only through the changing core FeO composition. NC models are straightforward to interpret and provide important context for the more complicated MOC cases, but are overly simplified. Middle-Out Crystallization (MOC) models generalise the basal magma ocean model of Labrosse et al. (2007) to account for FeO exchange with the core. As explained in section 2.2, this model does not represent the thermal boundary layer at the base of the mantle, which simplifies the calculation by tying together the core and mantle thermal evolution, but means that the heat released at the CMB by the exothermic reaction cannot be readily included in a self-consistent manner. Since a primary motivation for using the Labrosse et al. (2007) model is to compare results to existing solutions, we did not pursue more complex options, though this should be an avenue of future work. Another useful generalisation of the MOC model would be to include pressure dependence and allow the layer to deviate from the liquidus (Blanc et al., 2020).

In MOC models without FeO loss to the core the basal magma ocean can persist until the present day (Labrosse et al., 2007, and Fig. 2). This result has previously led to the suggestion that the BMO is related to the presence of Ultra-Low Velocity Zones at the base of Earth's present-day mantle (Labrosse et al., 2007, 2015), though recent work shows that the BMO can crystallize before the present day under certain conditions (Blanc et al., 2020). The addition of FeO loss causes the lifetime of the basal magma ocean to decrease from 3 Gyrs to 1 Gyr across the ranges $2 \leq P \leq 10$ and $0.02 \leq \bar{c}_{FeO}^m \leq 0.2$ considered here (Fig. 6a). However, while we have not obtained any MOC models with magma oceans that survive to the present-day, this does not indicate that such solutions do not exist because there are several parameters characterising the BMO thermal evolution that we have not varied. The assumptions described above will also influence the BMO evolution. Nevertheless, it seems reasonable to conclude that the addition of FeO loss to the core reduces the lifetime of the BMO.

MOC models with $P = 10$ and an initial bulk FeO concentration of 10% become gradually depleted in FeO over time (e.g. Fig. 3), raising the possibility that the BMO could become lighter than the overlying solid mantle. Such a scenario would presumably induce a rapid overturn of the whole system, thereby shortening the lifetime of the BMO compared to the estimates above. However, we cannot quantitatively assess this possibility because the composition of the solid mantle is not explicitly calculated in the Labrosse et al. (2007) model. Such a treatment would involve coupling the thermal evolution of the BMO to a model of the solid mantle, which is beyond the scope of the present study.

In both MOC and NC models there is substantial mass transfer across the CMB (Figs. 5 and 6), with fluxes much larger than values for the solid mantle (Buffett and Seagle, 2010; Davies et al., 2018) or the flux of light element down the core pressure gradient (Gubbins and Davies, 2013). This contrasts with the conventional picture that the core's light element inventory was set entirely during its formation (Rubie et al., 2015) and suggests that the present core O concentration may not provide a strong constraint for core formation models.

FeO transfers from the mantle to the core at all times in all NC models with $\bar{c}_{FeO}^m \geq 0.2$ and $P > 2$. In MOC models FeO transfers to the core for all parameter combinations we have tested. MOC models with $\bar{c}_{FeO}^m = 0.2$ and $P \leq 2$ show FeO transfer to the mantle during the first few hundred million years; however, estimated bulk magma ocean iron compositions of 10-20% (Andrault et al., 2012; Tateno et al., 2014) suggest that this scenario is unlikely to apply to Earth. The long timescale behaviour may be influenced by our assumption that P remains constant in time and hence does not vary with temperature T or liquid oxygen concentration $\bar{c}_O^c$. Thermal history models suggest a CMB temperature drop of over 1000 K over the last 4.5 Gyrs (Nimmo, 2015; Davies, 2015), while the chemical models in this paper show that $\bar{c}_O^c$ at the CMB increases significantly with time. There is general agreement that P decreases with decreasing T (e.g. Fischer et al., 2015; Pozzo et al., 2019); however, the dependence of P on composition is much harder to constrain. Davies et al. (2018) found that the partition coefficient between liquid iron and ferropericlase at CMB conditions increases with $\bar{c}_O^c$, which is consistent with the work of Fischer et al. (2015). Therefore the values of P used in this work (Pozzo et al., 2019), which were calculated at liquid oxygen concentrations of 5 mol%, are expected to decrease over time due to the falling temperature and increase over time due to rising liquid oxygen concentration; the effects will partly cancel. It is presently hard to estimate the degree of cancellation as there is still no clear picture of the temperature- and composition-dependence of P at CMB conditions. We therefore believe that adopting a time-independent P is a reasonable first approximation and that the long-time behaviour of our model is plausible.

If FeO were to transfer from the core to the mantle the dynamics may differ from those studied in this paper. FeO lost from the core would increase the density and stability of material at the base of the magma ocean, but would leave anomalously dense material at the top of the core. This material would be free to sink and thus the dynamics at the top of the core would not be purely diffusive as assumed here. The motion induced by sinking material should depend on whether the environment were stably stratified (e.g. due to a preceding episode of FeO transfer into the core) or neutrally buoyant (e.g. if the core were vigorously convecting throughout). The transition between these two distinct dynamical scenarios depends not just on P but on the properties of the chemical boundary layers above and below the CMB (in our simple model the key parameters are the bulk core and MO compositions, $\bar{c}_O^c$ and $\bar{c}_{FeO}^m$ respectively) and would be most likely to occur for

low values of P and $\bar{c}^m_{FeO}$ and high values of $\bar{c}^c_O$, i.e. times long after core formation. Based on values of $\bar{c}^m_{FeO} = 0.1 - 0.2$ we therefore speculate that FeO loss from the core, if it occurred at all, would arise long after core formation in an already stratified environment.

Flux of oxygen creates a stabilising compositional gradient at the top of the core. In NC models that span 4 Gyrs these layers are $120 - 150$ km-thick (Fig. 5d), which are thicker than previous estimates (Buffett and Seagle, 2010; Gubbins and Davies, 2013) and comparable to the estimated thickness proposed to explain periodic decadal fluctuations in the dipole field and core zonal flow (Buffett et al., 2016), though thinner than estimates from some seismic studies (Helffrich and Kaneshima, 2010; Kaneshima, 2017). The presence of a thick FeO-stratified layer is supported by the study of Brodholt and Badro (2017), who show that partitioning of FeO from the mantle into an Fe-Si-O core can also account for the observed slow seismic velocities while maintaining an overall density stratification. Oxygen is transferred across the layer by diffusion, with convection below the chemically stable layer mixing some light element to greater depths.

Heat released by the exothermic reaction is ≈ -0.1 to -50 TW in the first 1 Gyrs following core formation (Fig. 4). Core evolution models with high core conductivity predict minimum CMB heat flows of at least $\sim$20 TW are needed to sustain the early dynamo in the absence of FeO transfer (Nimmo, 2015; Davies et al., 2015) and so the predicted values of $Q_{\rm h}$ can potentially exceed the required heat flow on their own. The exothermic reaction together with a stable oxygen-rich layer, which reduces the size of the convecting region, could significantly increase the heat flow constraints on mantle convection imposed by high core thermal conductivity. Some mantle models predict that $40 - 50$ TW could be extracted from the core at early times (Nakagawa and Tackley, 2014; Driscoll and Bercovici, 2014), which is perhaps sufficient for sustaining the field, but lower heat flows would probably require additional power sources such as MgO precipitation (O'Rourke and Stevenson, 2016; Badro et al., 2018).

The saturation solubility of FeO in liquid iron at core conditions has not been calculated, but is expected to decrease as the core cools in line with predictions for MgO (O'Rourke and Stevenson, 2016; Badro et al., 2016) and SiO_2 (Hirose et al., 2017). The FeO concentration at the top of the core increases with time in our model and so it is possible that FeO could precipitate below the CMB at some stage in the core's history. However, FeO precipitation may not release significant gravitational energy for powering the dynamo because the environment is stably stratified rather than well-mixed: dense residual fluid might only fall a short distance in the stable layer before reaching the position of neutral stability.

5. Conclusions

We have presented a simple 1-dimensional model of FeO transfer between a long-lived magma ocean and the liquid core. The model extends previous work (Buffett and Seagle, 2010; Gubbins and Davies, 2013) by coupling the core oxygen concentration to the FeO flux through the chemical boundary layer at the base of the mantle. We have demonstrated the model behaviour across a broad range of physical conditions employing new determinations of the partitioning of FeO between iron alloys and silicate melts at core conditions (Pozzo et al., 2019).

Our results (summarised in Figs. 5 and 6) show that the top of the core is rapidly enriched to a pure FeO composition if the magma ocean persists for 0.5-1 Gyr after core formation. The stably stratified region at the top of the core that develops in this time is around 60-80 km thick and would exceed 100 km after 4 Gyrs of evolution. With the values of the partition coefficient $P \approx 10$ obtained by Pozzo et al. (2019) and a bulk magma ocean FeO content of $\sim 10\%$, around 15-50% of the present day core oxygen content can be transferred across the core-mantle boundary in the first 1 Gyr. FeO loss to the core shortens the lifetime of a basal magma ocean such that, in all of our calculations, the BMO does not survive to the present day.

Declaration of competing interest

The authors declare that they have no known competing financial interests or personal relationships that could have appeared to influence the work reported in this paper.

Acknowledgements

CD acknowledges a Natural Environment Research Council personal fellowship, reference NE/L011328/1. DA and MP are supported by Natural Environment Research Council grant numbers NE/M000990/1 and NE/R000425/1.

Appendix A. Heat of reaction at the core-mantle boundary

Core evolution models generally assume that no mass is exchanged between the core and mantle (Nimmo, 2015); this constraint is to be relaxed here. The local energy equation, averaged over timescales associated with dynamo and convective processes, is (Gubbins et al., 2003)

$$\frac{\partial}{\partial t}\left[\rho(E+\frac{u^2}{2})\right]+\nabla\cdot\left[\rho(E+\frac{u^2}{2}+\frac{P}{\rho})\mathbf{u}+\mathbf{q}\right]+\rho\mathbf{u}\cdot\mathbf{F}=0, \quad \text{(A.1)}$$

where ρ is density, E is internal energy, $\mathbf{u}$ is the velocity, P is pressure (not to be confused with the partition coefficient used in the main text), $\mathbf{q}$ is the heat flux vector, $\mathbf{F}$ represents body forces acting on the fluid, and radiogenic heating has been omitted. Following standard procedures (Loper and Roberts, 1980), equation (A.1) is to be integrated over a penny-shaped disc of volume V straddling the CMB. Assuming that the CMB does not move with time (i.e. ignoring the slow contraction of the core, which makes a small contribution to the energy balance (Gubbins et al., 2003)) we have, for some scalar X,

$$\int \frac{\partial X}{\partial t} \mathrm{d}V = \frac{\mathrm{d}}{\mathrm{d}t}\int X \mathrm{d}V. \quad \text{(A.2)}$$

Assuming no surface masses or charges and continuity of stresses across the CMB gives

$$\oint\left[\rho(E+\frac{u^2}{2}+\frac{P}{\rho})\mathbf{u}+\mathbf{q}\right]\cdot\mathrm{d}\mathbf{A}=0, \quad \text{(A.3)}$$

where $\mathrm{d}\mathbf{A}$ is the area element on the surface of V. Defining $\mathbf{n}$ as the unit vector pointing radially outwards and noting that $\mathrm{d}\mathbf{A} = \mathbf{n}\mathrm{d}A$ on the upper surface and $\mathrm{d}\mathbf{A} = -\mathbf{n}\mathrm{d}A$ on the lower surface of V gives

$$\oint\left\langle\rho(E+\frac{u^2}{2}+\frac{P}{\rho})\mathbf{u}+\mathbf{q}\right\rangle\cdot\mathbf{n}\mathrm{d}A=0, \quad \text{(A.4)}$$

where $\langle X\rangle = X^c - X^m$, i.e. the difference between evaluating X directly below and above the CMB. Since we do not allow penetration of core fluid into the mantle or vice verse, $\mathbf{n}\cdot\mathbf{u}^m = \mathbf{n}\cdot\mathbf{u}^c = 0$ and continuity at the CMB requires $\mathbf{n}\cdot\langle\mathbf{q}\rangle = 0$. Here

$$q = -k\nabla T + \left(\mu - (\partial\mu/\partial T)_{P,T}T\right)\mathbf{i} \quad \text{(A.5)}$$

is the heat flux vector (Loper and Roberts, 1980) where k is the thermal conductivity, T is temperature, μ is the chemical potential,

and $\mathbf{i}$ is the mass flux vector. Defining $R_{FeO} = \mu - (\partial\mu/\partial T)_{P,T} T$ we have

$$\oint \mathbf{n} \cdot \langle -k \nabla T \rangle \, \mathrm{d}A = - \oint \mathbf{n} \cdot \langle R_{FeO} \mathbf{i} \rangle \, \mathrm{d}A. \quad \text{(A.6)}$$

Defining $Q^j = -\mathbf{n} \cdot k^j \nabla T^j \mathrm{d}A$ for $j = c, m$ and noting that $\mathbf{n} \cdot \langle \mathbf{i} \rangle = 0$ on the CMB gives

$$Q^m = Q^c - \oint \mathbf{n} \cdot \langle R_{FeO} \rangle \mathbf{i} \mathrm{d}A = Q^c - 4\pi r_{\mathrm{cmb}}^2 | \langle R_{FeO} \rangle \mathbf{i} |. \quad \text{(A.7)}$$

The second equality follows because $\langle R_{FeO} \rangle < 0$ (recalling that this is mantle value minus core value) and $\mathbf{n} \cdot \mathbf{i} < 0$ (mass flux is into the core). The heat of reaction, $Q_{\mathrm{h}} = -4\pi r_{\mathrm{cmb}}^2 | \langle R_{FeO} \rangle \mathbf{i} |$ is a heat sink that reduces the heat flowing through the lower mantle boundary layer compared to the heat flowing out of the core.

References

Alfè, D., Gillan, M., Price, G., 2002. Composition and temperature of the Earth's core constrained by combining ab initio calculations and seismic data. Earth Planet. Sci. Lett. 195, 91–98.

Andrault, D., Petitgirard, S., Lo Nigro, G., Devidal, J.-L., Veronesi, G., Garbarino, G., Mezouar, M., 2012. Solid-liquid iron partitioning in Earth's deep mantle. Nature 487 (7407), 354–357.

Badro, J., Aubert, J., Hirose, K., Nomura, R., Blanchard, I., Borensztajn, S., Siebert, J., 2018. Magnesium partitioning between Earth's mantle and core and its potential to drive an early exsolution geodynamo. Geophys. Res. Lett. 45, 13–24.

Badro, J., Côté, A., Brodholt, J., 2014. A seismologically consistent compositional model of Earth's core. Proc. Natl. Acad. Sci. 111, 7542–7545.

Badro, J., Siebert, J., Nimmo, F., 2016. An early geodynamo driven by exsolution of mantle components from Earth's core. Nature 536 (7616), 326.

Blanc, N., Stegman, D., Ziegler, L., 2020. Thermal and magnetic evolution of a crystallizing basal magma ocean in Earth's mantle. Earth Planet. Sci. Lett. 534, 116085.

Boukaré, C.-E., Ricard, Y., Fiquet, G., 2015. Thermodynamics of the MgO-FeO-SiO2 system up to 140 GPa: application to the crystallization of Earth's magma ocean. J. Geophys. Res. 120 (9), 6085–6101.

Braginsky, S., 1963. Structure of the F layer and reasons for convection in the Earth's core. Sov. Phys. Dokl. 149, 8–10.

Braginsky, S., 1993. MAC-oscillations of the hidden ocean of the core. J. Geomagn. Geoelectr. 45, 1517–1538.

Breuer, D., Moore, W., 2015. Dynamics and thermal history of the terrestrial planets, the Moon, and Io. In: Schubert, G. (Ed.), Treatise on Geophysics, Second Edition, vol. 10. Elsevier, Amsterdam, pp. 255–305.

Brodholt, J., Badro, J., 2017. Composition of the low seismic velocity E' layer at the top of Earth's core. Geophys. Res. Lett. 44, 2017GL074261.

Buffett, B., 2014. Geomagnetic fluctuations reveal stable stratification at the top of the Earth's core. Nature 507, 484–487.

Buffett, B., Knezek, N., Holme, R., 2016. Evidence for MAC waves at the top of Earth's core and implications for variations in length of day. Geophys. J. Int. 204, 1789–2000.

Buffett, B., Seagle, C., 2010. Stratification of the top of the core due to chemical interactions with the mantle. J. Geophys. Res. 115, B04407.

Chidester, B.A., Rahman, Z., Righter, K., Campbell, A.J., 2017. Metal-silicate partitioning of U: Implications for the heat budget of the core and evidence for reduced U in the mantle. Geochim. Cosmochim. Acta 199, 1–12.

Davies, C., 2015. Cooling history of Earth's core with high thermal conductivity. Phys. Earth Planet. Inter. 247, 65–79.

Davies, C., Pozzo, M., Gubbins, D., Alfè, D., 2015. Constraints from material properties on the dynamics and evolution of Earth's core. Nat. Geosci. 8, 678–687.

Davies, C., Pozzo, M., Gubbins, D., Alfè, D., 2018. Partitioning of oxygen between ferropericlase and Earth's liquid core. Geophys. Res. Lett. 45, 6042–6050.

de Koker, N., Steinle-Neumann, G., Vojtech, V., 2012. Electrical resistivity and thermal conductivity of liquid Fe alloys at high P and T and heat flux in Earth's core. Proc. Natl. Acad. Sci. 109, 4070–4073.

Driscoll, P., Bercovici, D., 2014. On the thermal and magnetic histories of Earth and Venus: influences of melting, radioactivity, and conductivity. Phys. Earth Planet. Inter. 236, 36–51.

Du, Z., Jackson, C., Bennett, N., Driscoll, P., Deng, J., Lee, K., Greenberg, E., Prakapenka, V., Fei, Y., 2017. Insufficient energy from MgO exsolution to power early geodynamo. Geophys. Res. Lett. 4, 2017GL075283.

Dziewonski, A., Anderson, D., 1981. Preliminary reference Earth model. Phys. Earth Planet. Inter. 25, 297–356.

Fischer, R.A., Nakajima, Y., Campbell, A.J., Frost, D.J., Harries, D., Langenhorst, F., Miyajima, N., Pollok, K., Rubie, D.C., 2015. High pressure metal-silicate partitioning of Ni, Co, V, Cr, Si, and O. Geochim. Cosmochim. Acta 167 (Supplement C), 177–194.

Frost, D., Asahara, Y., Rubie, D., Miyajima, N., Dubrovinsky, L.S., Holzapfel, C., Ohtani, E., Miyahara, M., Sakai, T., 2010. Partitioning of oxygen between the Earth's mantle and core. J. Geophys. Res. 115, B02202.

Gomi, H., Ohta, K., Hirose, K., Labrosse, S., Caracas, R., Verstraete, V., Hernlund, J., 2013. The high conductivity of iron and thermal evolution of the Earth's core. Phys. Earth Planet. Inter. 224, 88–103.

Gubbins, D., Alfe, D., Masters, G., Price, G., Gillan, M., 2003. Can the Earth's dynamo run on heat alone? Geophys. J. Int. 155, 609–622.

Gubbins, D., Davies, C., 2013. The stratified layer at the core-mantle boundary caused by barodiffusion of oxygen, sulphur and silicon. Phys. Earth Planet. Inter. 215, 21–28.

Helffrich, G., Kaneshima, S., 2010. Outer-core compositional stratification from observed core wave speed profiles. Nature 468, 807–809.

Hirose, K., Labrosse, S., Hernlund, J., 2013. Compositional state of Earth's core. Annu. Rev. Earth Planet. Sci. 41, 657–691.

Hirose, K., Morard, G., Sinmyo, R., Umemoto, K., Hernlund, J., Helffrich, G., Labrosse, S., 2017. Crystallization of silicon dioxide and compositional evolution of the Earth's core. Nature 543 (7643), 99–102.

Kaneshima, S., 2017. Array analysis of SmKS waves and stratification of Earth's outermost core. Phys. Earth Planet. Inter. 223, 2–7.

Konôpková, Z., McWilliams, R., Gómez-Pérez, N., Goncharov, A., 2016. Direct measurement of thermal conductivity in solid iron at planetary core conditions. Nature 534, 99–101.

Labrosse, S., Hernlund, J., Coltice, N., 2007. A crystallizing dense magma ocean at the base of the Earth's mantle. Nature 450, 866–869.

Labrosse, S., Hernlund, J.W., Hirose, K., 2015. Fractional melting and freezing in the deep mantle and implications for the formation of a basal magma ocean. In: Badro, J., Walter, M. (Eds.), The Early Earth: Accretion and Differentiation. AGU. Ch. 7.

Loper, D., Roberts, P., 1980. On the motion of an iron-alloy core containing a slurry: II. A simple model. Geophys. Astrophys. Fluid Dyn. 16, 83–127.

Masters, G., Gubbins, D., 2003. On the resolution of density within the Earth. Phys. Earth Planet. Inter. 140, 159–167.

Nakagawa, T., Tackley, P., 2014. Influence of combined primordial layering and recycled MORB on the coupled thermal evolution of Earth's mantle and core. Geochem. Geophys. Geosyst. 15, 619–633.

Nimmo, F., 2015. Energetics of the core. In: Schubert, G. (Ed.), Treatise on Geophysics, Second Edition, vol. 8. Elsevier, Amsterdam, pp. 27–55.

Nimmo, F., Price, G., Brodholt, J., Gubbins, D., 2004. The influence of potassium on core and geodynamo evolution. Geophys. J. Int. 156, 363–376.

O'Rourke, J., Korenaga, J., Stevenson, D., 2017. Thermal evolution of Earth with magnesium precipitation in the core. Earth Planet. Sci. Lett. 458, 263–272.

O'Rourke, J.G., Stevenson, D.J., 2016. Powering Earth's dynamo with magnesium precipitation from the core. Nature 529 (7586), 387–389.

Pozzo, M., Davies, C., Gubbins, D., Alfè, D., 2012. Thermal and electrical conductivity of iron at Earth's core conditions. Nature 485, 355–358.

Pozzo, M., Davies, C., Gubbins, D., Alfè, D., 2013. Transport properties for liquid silicon-oxygen-iron mixtures at Earth's core conditions. Phys. Rev. B 87, 014110.

Pozzo, M., Davies, C., Gubbins, D., Alfè, D., 2019. The FeO content of Earth's core. Phys. Rev. X 9, 041018.

Ribe, N., 1998. Spouting and planform selection in the Rayleigh–Taylor instability of miscible viscous fluids. J. Fluid Mech. 377, 27–45.

Rubie, D., Nimmo, F., Melosh, H., 2015. Formation of Earth's core. In: Schubert, G. (Ed.), Treatise on Geophysics, Second Edition, vol. 9. Elsevier, Amsterdam, pp. 43–79.

Solomatov, V., 2015. Magma oceans and primordial mantle differentiation. In: Schubert, G. (Ed.), Treatise on Geophysics, Second Edition, vol. 10. Elsevier, Amsterdam, pp. 81–104.

Tateno, S., Hirose, K., Ohishi, Y., 2014. Melting experiments on peridotite to lowermost mantle conditions. J. Geophys. Res. 119, 4684–4694.

Xu, J., Zhang, P., Haule, K., Minar, J., Wimmer, S., Ebert, H., Cohen, R., 2018. Thermal conductivity and electrical resistivity of solid iron at Earth's core conditions from first principles. Phys. Rev. Lett. 121 (9), 096601.

Ziegler, L.B., Stegman, D.R., 2013. Implications of a long-lived basal magma ocean in generating Earth's ancient magnetic field. Geochem. Geophys. Geosyst. 14, 4735–4742.